FAILURE ANALYSIS OF PUMP SHAFT USED IN OIL EXTRACTION PLATFORMS

Danilo Borges Villarino de Castro, danilobvc@yahoo.com.br
Jéferson Aparecido Moreto, jeferson_moreto@yahoo.com.br
Otávio Contart Gamboni, otaviocgamboni@yahoo.com.br
Dirceu Spinelli, dspinell@sc.usp.br
José Ricardo Tarpani, jrpan@sc.usp.br
Department of Materials, Aeronautics and Automotive Engineering, Engineering School of São Carlos / University of São Paulo – Av. Trabalhador Sãocarlense, 400; Parque Arnold Schmidt, São Carlos-SP; Brazil

Abstract. *This study investigates the possible causes of the failure of a horizontal centrifugal pump shaft used in coastal oil extraction platforms. The rotating shaft in question broke in service under normal operational conditions of the equipment during brackish water pumping for enhancing oil well extraction. Brackish water was reported as not containing a significant amount of hydrogen sulfide (H_2S), as typically resulting from seaweed decomposition. The shaft material was UNS S31803 duplex austenoferritic stainless steel supplied in the forged condition. A 24 mm long carbon steel nut was threaded to the shaft in the fractured region. Chemical analysis, hardness measurements and metallographic and fractographic inspections were carried out. It has been concluded that the pump shaft ruptured by sub-critical fatigue crack growth. Two cracks nucleated simultaneously at the root of two neighbor fillets, with extensive spread of the main crack leading to the complete fracture of the component. The poor quality of the root fillet finishing led to a massive presence of stress raisers, such as sharp edges and corners, scratches and notch-type defects, which were identified as the main cause of failure.*

Keywords*: centrifugal pump shaft, failure analysis, oil-drilling platform.*

1. INTRODUCTION

UNS S31803 duplex austoferritic steel has been applied to pumps, valves, chokes, Xmas trees, pipeworks/flanges, bolting, connectors and manifolds, in oil and industrial gas. UNS S31803 is described as duplex stainless steel with a microstructure of 50:50 austenite and ferrite. The steel combines good mechanical strength (typically up to above 480 MPa yield strength) and ductility with moderate to good corrosion resistance in a variety of environments. By agreement, the alloy can be supplied with PREn (Pitting Resistance Equivalent) at > 34, ensuring that the resistance to pitting is a high as possible for this alloy grade. In addition, the steel offers good resistance to stress corrosion cracking. These attributes mean that this duplex steel can be successfully used as an alternative to 300 series stainless steels in applications to which higher mechanical strength/lower weight and/or resistance to stress corrosion cracking are required (UNS S31803, 2007).

Pumps are machines used to perform billets that displace a liquid through flow. Being engine generators, they transform the mechanical work of the energy into their flow functioning, which is communicated to the liquid in the forms of pressure and kinetic energy. Some authors call them hydraulic machine tools, because they perform useful work to move a particular liquid. Pumps are used in hydraulic circuits to convert mechanical energy into hydraulic energy. The mechanical action creates a partial vacuum in the pump inlet, which allows the atmospheric pressure to force fluid from the tank through the suction line to enter the pump (Brasil, 2010).

The damaged part or the whole equipment is almost always replaced when a pump fails without an analysis of the reason of failure. Whatever the correct action, it is frequently a temporary solution, and the likelihood of pump failure is high for the same reason. Due to the high cost of maintenance, parts and profit, this practice of simple exchange is no longer acceptable. There are many broad categories of causes of failures in centrifugal pumps: wrong design, defective material, poor workmanship, poor installation/assembly, use under abnormal conditions, and improper operation (Veritatis Verri, 2010).

During operation, pump shafts usually suffer from degradation as a result of corrosion and/or mechanical degradation, usually in the form of fatigue failures. In many cases corrosion precedes fatigue failure and can actually accelerate the rate of failure. Pump shafts are generally exposed to the liquid being pumped either on a continual basis or at certain locations along the length of the shaft (Berndt, 2001).

Alduqri studied the centrifugal pump used to pump the petrol mixture to the separators of refinery; the failure results in a fire of the refinery. The pump has been installed on May 1979. The pump is start up at 2,975 rpm for 14 hours with a 2-hour complete shut-down interval and normally operates 6 days a week throughout the year. The pump was tripped and started for 12 times for around 12 hours. The failure incident occurred on 30/07/2010 at 8:00 PM. The main contribution to the failure is the life of the shaft exceeded its fatigue limit and also the combined action of environment, geometry and stresses could be one of the causes of the crack initiation at the failure location. The propagation stage might be resulted by corrosion fatigue. The final stage resulted by mechanical stresses (Alduqri, 2010).

In short, the aim of this study is to investigate the possible causes of the failure of a horizontal centrifugal pump shaft used in coastal oil extraction platforms.

2. MATERIALS AND METHODS

This study investigated the failure analysis of a rotating shaft of a centrifugal pump injection, located in an oil drilling platform. This rotating shaft broke in service under normal operating conditions of the injection pump during the pumping of brackish water wells for oil drilling on coasts. It is known that water in the operating component does not contain a significant amount of hydrogen sulfide (H_2S) generated during the decomposition of seaweed.

The shaft material is an austenoferritic duplex stainless steel, classification UNS S31803, supplied in forged condition. In the region of fracture of the shaft, there was a nut threaded carbon steel of approximately 24.0 mm length.

Rockwell hardness measurements on the B scale (HRB) were taken in five different positions in the cross-section of the shaft in a parallel plane close to the fracture of the part, according to standard ASTM E-18-08.

Metallographic polished surfaces, corresponding to the longitudinal shaft fracture, were observed with and without chemical attack in an Olympus BX60M optical microscope. They were embedded in a conductive bakelite and sanded with sandpaper water with particle sizes #80, 120, 220, 400, 600, 800, 1200, and 2000. The sanded surfaces were then polished in three stages: the first with chromium dioxide, the second solution with alumina 0.3 μm, and the final stage with a solution of 0.05 μm alumina. The chemical attack was carried out with nitromuriatic acid, consisting of a mixture of 8 mL of concentrated nitric acid, 12 mL of concentrated sulfuric acid and 1000 mL of ethanol.

The microstructure of the material was analyzed via DSM 960 ZEISS scanning electron microscopy (SEM) to determine its phases and to qualify the chemical composition of the present precipitates through energy dispersive spectroscopy (EDS).

3. RESULTS AND DISCUSSIONS

The material's chemical composition is provided in Tab. 1. Except for chromium, all other chemical elements are in accordance with the specifications for UNS S31803 steel.

Table 1. Materials' chemical composition (wt%).

Chemical elements	C	Si	Mn	Cr	Ni	Mo	P	S
Nominal	0.03 (max)	1.00 (max)	2.00 (max)	21.0 – 23.0	4.5 – 6.5	2.5 – 3.5	0.035 (max)	0.015 (max)
Measured	0.04	0.44	0.96	24.02	5.10	3.22	0.017	0.012

Regarding the hardness tests, a value of (94.8 ± 2.0) HRB, compatible with the material analyzed (maximum of 104 HRB), was obtained.

Fig. 3 shows two views of the fractured shaft profile. It is possible to observe that two cracks propagate in parallel, one over the other, leading to complete fracture of the component.

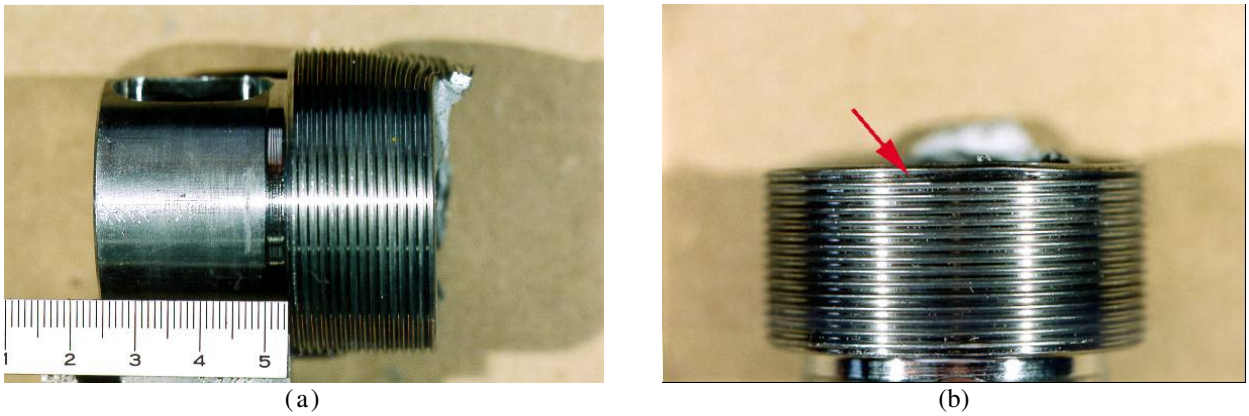

(a) (b)

Figure 3. (a) Profile of the fractured shaft. (b) The red arrow indicates the main crack parallel to the cross-section of the component

In Fig. 4, the red arrows indicate the nucleation sites of the secondary (Fig. 4(a)) and main (Fig. 4(b)) fatigue cracks shown in Fig. 3.

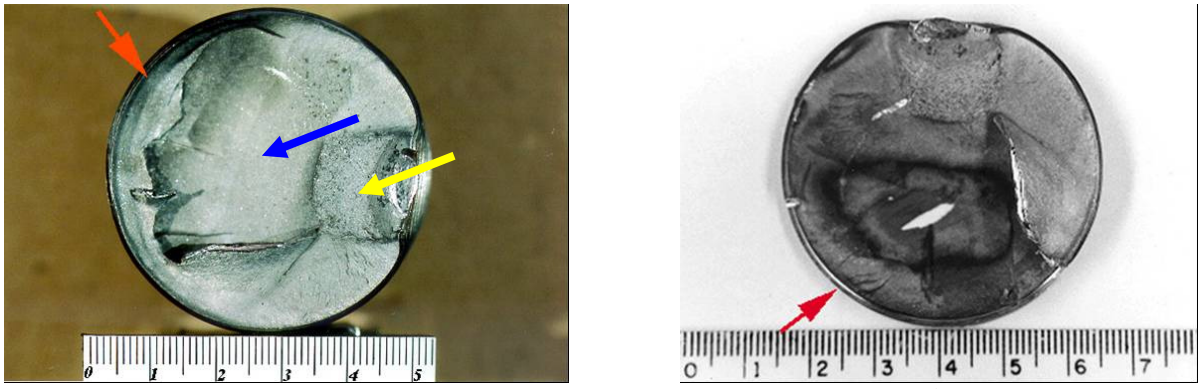

(a) (b)

Figure 4. Sites of initiation of fatigue cracks indicated by red arrows: (a) secondary cracks and (b) main crack

The presence of beach marks on the fracture surface of the shaft, indicated by a blue arrow in Fig. 4(a), demonstrates that the axle broke under the fatigue mechanism. In the same figure, the yellow arrow points to the remaining section of the shaft, which fractured catastrophically when the applied stress exceeded the strength of the material. The small remainder of this section shows the relatively low voltages at which the component was subjected in service. This type of fracture is similar to that shown in studies of Muhammad and Deen (Muhammad, 2010).

Fig. 5 shows the microstructure of steel that makes up the fractured shaft, confirming the development of a duplex structure. The micrograph shows the ferrite (indicated by a blue arrow) and austenite (a red arrow), typical of this steel in the solubilized state. There is also a high texturing of the steel structure in the longitudinal direction of the axis, indicating a high degree of deformation experienced by the material during hot work.

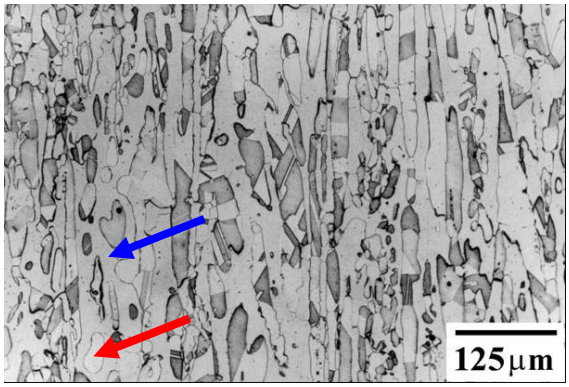

Figure 5. Microstructure of the studied steel

Fig. 6 shows two views of the same metallographic sample respectively with and without chemical attack, identifying the exact point of rupture of the shaft located at the bottom of the fillet and indicated by yellow arrows. The green arrows point to the bottom fillet closest to that fractured components in service.

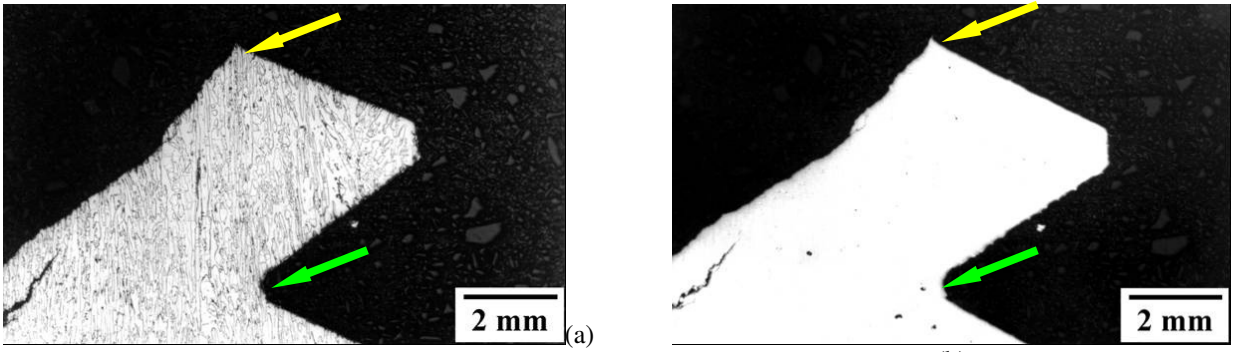

(a) (b)

Figure 6. Two views of the fractured fillet profile indicated by yellow arrows: (a) with etching and (b) without chemical attack

An expansion of this thread is shown in Fig. 7, where the blue arrows point to two preferred points of stress concentration in the form of sharp edges or corners, placed on the shaft during the machining process of the fillet. Returning to Fig. 6, one can conclude that the fatigue crack which completely fractured the left edge shaft started in the lower profile of the fillet.

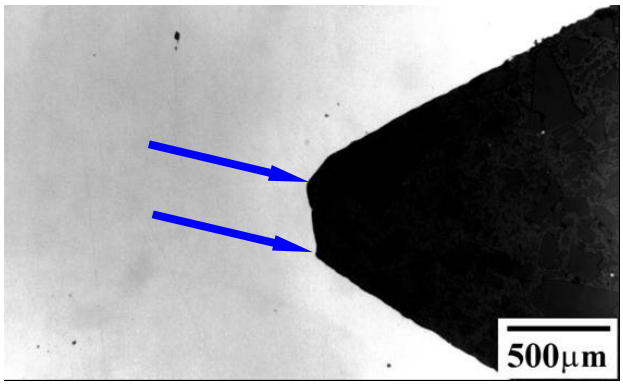

Figure 7. Detail of the bottom of the fillet neighbor which broke in service (without etching)

Fig. 8 shows a sequence of magnifications of an edge (indicated by red arrows) similar to that in which the fatigue crack nucleates in the shaft fracture.

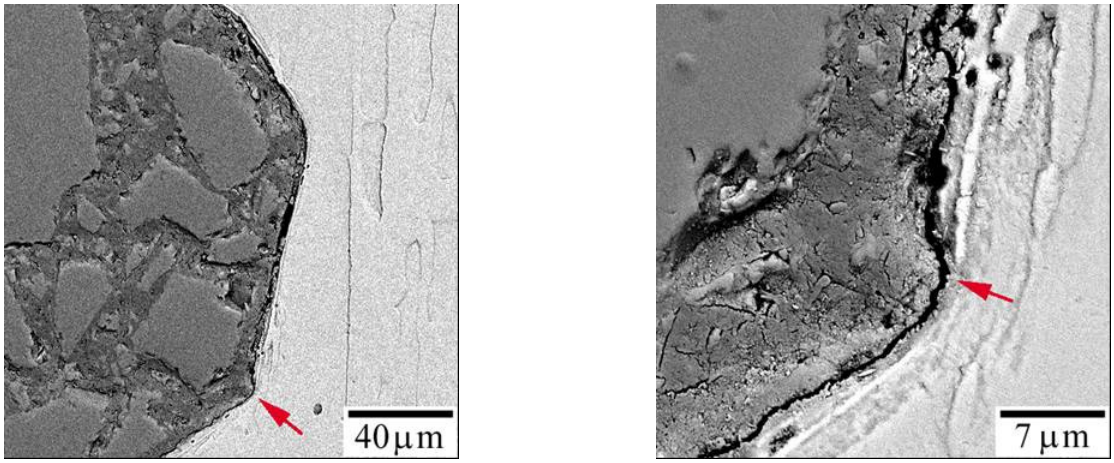

(a) (b)

Figure 8. Sequence of SEM pictures detailing the site of fatigue crack nucleation (red arrows) on the shaft fractured in service (sample with chemical attack). Images obtained with back-scattered electron

Fig. 9 depicts the site of fatigue fracture indicated by the yellow arrow.

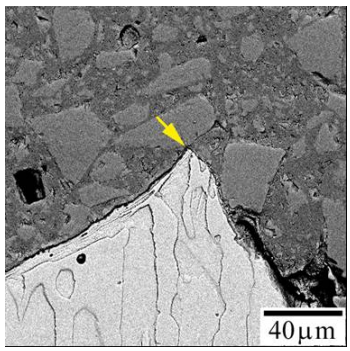

Figure 9. Site of fracture indicated by the yellow arrow (sample with chemical attack). Image obtained with back-scattered electron

Using SEM, it was possible to identify and characterize in detail the nucleation sites of the broken minor and major cracks, previously shown in Fig. 4. As shown in Fig. 10, the secondary fatigue crack was nucleated near the root of the fillet, more precisely in an inclusion present in that location. The micro-chemical analysis allowed identifying a second phase, probably a particle of iron carbide and chromium.

Fig. 11 shows that the main fatigue crack nucleation occurred exactly at the bottom of the fillet, which appears highly irregular, with the presence of indiscriminate risks and defects of the notch. Fig. 12 illustrates the patterns of rifling through both minor and major fatigue cracks developed.

Through a microprobe operating with energy dispersive X-ray, which equips the scanning electron microscope, the particle of the second phase that originated the secondary fatigue crack, shown in Fig. 10, was chemically analyzed. Fig. 13 depicts the absorption spectrum of the particle, which allows identifying peaks of the absorption of elements Fe, Cr and C. Other elements present in the composition of the steel matrix, which involves the particles analyzed, also show their characteristic peaks.

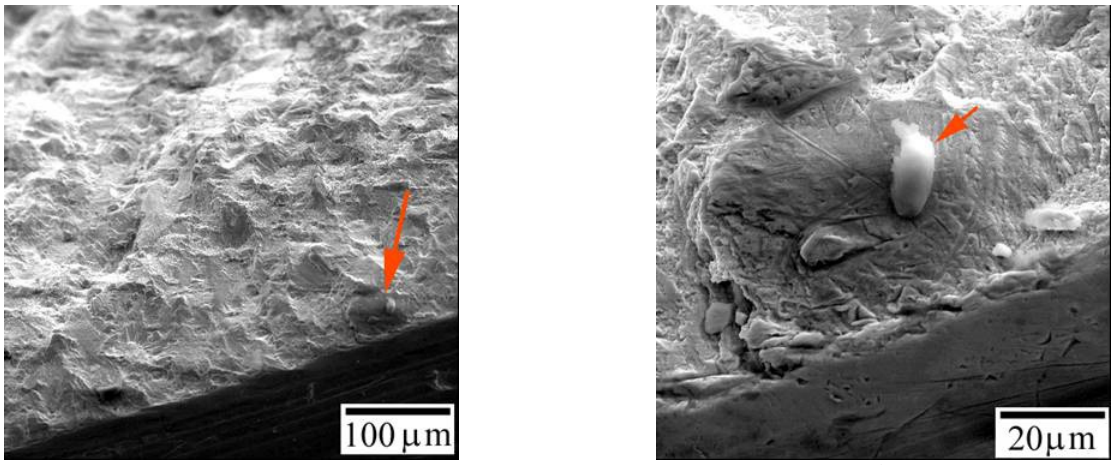

(a) (b)

Figure 10. Details of the site of initiation of secondary fatigue crack nucleated at an inclusion (red arrows) the root of the fillet

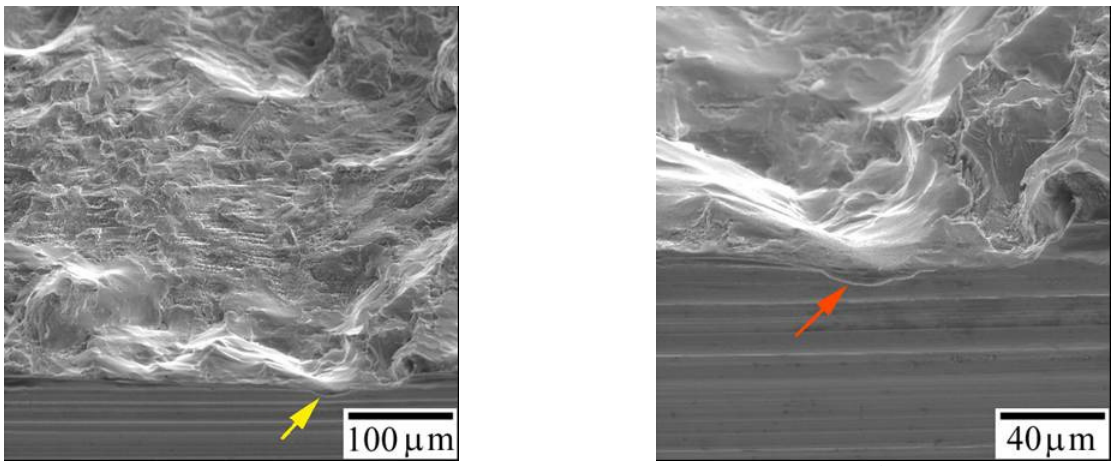

(a) (b)

Figure 11. Details of the site of initiation of the main crack from fatigue nucleated on the bottom edge of the bead machined in the shaft (yellow and red arrows, respectively)

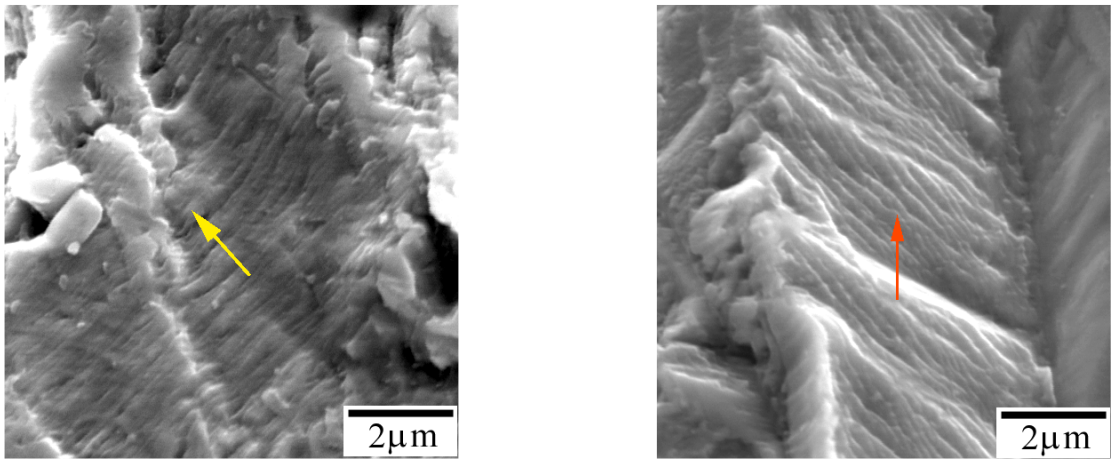

(a) (b)

Figure 12. Patterns of fatigue rifling developed on the fracture surface during the progress of cracks: (a) secondary and (b) main. Arrows indicate direction and location of the crack growth

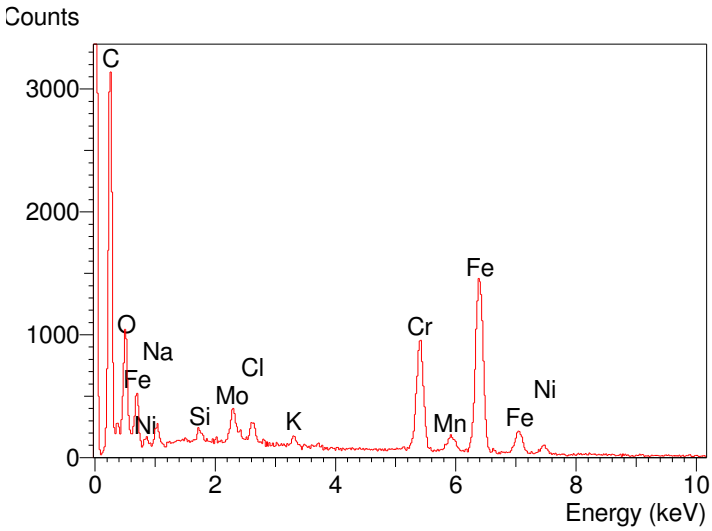

Figure 13. Absorption spectrum of the particle that caused the secondary fatigue crack

4. CONCLUSIONS

After the whole sequence of failure analysis of the fractured shaft, it was concluded that the injection pump shaft broke in service by the mechanism of subcritical fatigue crack growth. Two cracks were nucleated simultaneously at the root fillets of two neighbors, with the extensive propagation of the main crack leading to a complete fracture of the component. The poor quality of the interior finish in the fillet, with the massive presence of stress concentrators, such as sharp edges or corners, scratches and defects of the notch, was identified as the main cause of failure.

Based on these results, a stricter control of the machining process of the fillets should be adopted. A change in the process of introduction of fillet into the shaft, for example, opting for rolling the fillets instead of their machining, could lead to a better performance of the service provided that a suitable quality control is also implemented for the new procedure.

5. ACKNOWLEDGEMENTS

The authors would like to acknowledge the Materials, Aeronautics and Automotive Engineering Department of Engineering School of São Carlos – USP for granting us the use of its facilities.

6. REFERENCES

Alduqri, Y.A.A., 2010. “Case study report: failure analysis of centrifugal pump shaft”. Universiti Teknologi Malaysia (UTM), Nov 23 2010, 11p.

Berndt, F., Bennekom, A. "Pump shaft failures - a compendium of case studies". Engineering Failure Analysis, v.8, 2001, p. 135-144.

Brasil, A.N. "Bombas – classificação e descrição". Máquinas Termohidráulicas de Fluxo, Chapter 3, 1 Feb. 2010, p. 62-91.

Muhammad, W., Deen, K.M. "Failure analysis of water pump shaft". Journal of Failure Analysis and Prevention, v.10, 2010, p. 161-166.

UNS S31803. "UNS S31803/1.4622/F51 Data sheet". Smiths High Performance, 2007, 1p.

Verri Veritatis. "Análise de causas básicas – bombas centrífugas". Verri Veritatis Consultoria Ltda, 5 Jan. 2010, <www.verriveritatis.com.br>.

7. RESPONSIBILITY NOTICE

The authors are responsible for the printed material included in this paper.